281

Stress wave emission and cavitation bubble dynamics by nanosecond optical breakdown in a tissue phantom

By EMIL-ALEXANDRU BRUJAN† AND ALFRED VOGEL‡

Institute of Biomedical Optics, University of Lübeck, Peter-Monnik-Weg 4, 23564 Lübeck, Germany

Stress wave emission and cavitation bubble dynamics after optical breakdown in water and a tissue phantom with Nd : YAG laser pulses of 6 ns duration were investigated both experimentally and numerically to obtain a better understanding of the physical mechanisms involved in plasma-mediated laser surgery. Experimental tools were high-speed photography with 50 000 frames s^{-1}, and acoustic measurements. The tissue phantom consisted of a transparent polyacrylamide (PAA) gel, the elastic properties of which can be controlled by modifying the water content. Breakdown in water produced a purely compressive stress wave. By contrast, in stiff PAA samples and for sufficiently large pulse energies, the compression wave was followed by an intense tensile wave, similar to the behaviour previously observed in cornea. The elastic/plastic response of the medium led to a significant decrease of the maximum size of the cavitation bubble and to a shortening of its oscillation period which was found to be related to the generation of the tensile stress wave upon breakdown. For increasing elastic modulus of the PAA, both the amplitudes of the bubble oscillation and of the stress wave emitted during bubble collapse decreased until the bubble oscillation was so strongly damped that no collapse stress wave was emitted. Numerical simulations were performed using a spherical model of bubble dynamics which includes the compressibility and elastic/plastic behaviour of the medium, viscosity, density and surface tension. The calculations revealed that consideration of the elastic/plastic behaviour of the medium surrounding the bubble is essential to describe the experimentally observed bipolar shape of the stress wave emitted upon optical breakdown. Water is a poor tissue model because the shape of the emitted stress waves and the bubble dynamics differ strongly for both materials. The mechanical properties of PAA were also found to be quite different from those of tissues. Experimental and numerical results provided evidence that the dynamic mechanical properties relevant for optical breakdown in PAA and tissue differ by as much as two orders of magnitude from the static values. The discovery of a tensile stress wave after optical breakdown in tissue-like media is of great importance for the assessment of collateral damage in laser surgery because biological tissues are much more susceptible to tensile stress than to compressive stress.

1. Introduction

With the widespread use of lasers in medical and commercial applications, a physical understanding of the interaction between the laser pulse and absorbing

† Present address: Department of Hydraulics, University Politehnica, Spl. Independentei 313, 060042 Bucharest, Romania. eabrujan@yahoo.com.
    ‡ Author to whom correspondence should be addressed. vogel@bmo.uni-luebeck.de.

medium is both desirable and necessary. These investigations are of interest from a practical point of view, but also of significant interest in terms of the basic physics involved in the nonlinear interplay of optical and acoustic phenomena. Light can affect materials through diverse means including electronic, chemical, thermal and mechanical processes. A particular electronic and thermomechanical process is the optical breakdown which involves generation of plasma by multiphoton and avalanche ionization followed by explosive vaporization and mechanical expansion (Vogel *et al.* 1996*a*, *b*; Lauterborn *et al.* 1999). Optical breakdown occurs at locations where the irradiance is sufficiently high to produce a critical free-electron density of about 10^{21} cm^{-3} (Shen 1984; Noack & Vogel 1999). The fast energy deposition during optical breakdown causes a rapid temperature and pressure rise within the plasma, leading to its explosive expansion. The energy densities reached after nanosecond optical breakdown are in the order of 30–40 kJ cm^{-3} (Vogel *et al.* 1996*a*, 1999*a*), corresponding to a peak temperature of about 10000 K (Stolarski *et al.* 1995) and an initial plasma pressure of 2–7 Gpa, depending on the pulse energy (Vogel *et al.* 1996*a*, 1999*a*). Therefore, plasma expansion is a vigorous event accompanied by a sequence of shock wave emission and cavitation bubble generation.

In recent years, the interaction of pulsed laser light with biological tissues has been the object of extensive research (Vogel & Venugopalan 2003), and laser-induced stress wave and bubble formation in tissues or tissue phantoms have been investigated in various studies (Vogel *et al.* 1986, 1990, 1994*a*, *b*, 1996*a*, 1999*b*; Dyer, Khosroshahi & Tuft 1993; van Leeuwen *et al.* 1993; Ith *et al.* 1994; Juhasz *et al.* 1994, 1996; Brinkmann *et al.* 1996; Jansen *et al.* 1996; Asshauer *et al.* 1997; Delacretaz & Walsh 1997; Frenz *et al.* 1998; Brujan *et al.* 2001*a*, *b*; Venugopalan *et al.* 2002). This interest was motivated by the increasingly important role of cavitation and associated bubble dynamics in medical applications. Whenever short laser pulses are used to ablate, cut, or disrupt tissue inside the human body, cavitation bubbles are produced that interact with the tissue. This situation is encountered in various applications of laser surgery, such as intraocular photodisruption (Vogel *et al.* 1986, 1990, 1994*b*), intrastromal corneal refractive surgery (Vogel *et al.* 1997; Juhasz *et al.* 1999), laser-assisted keratomileusis (Krueger *et al.* 1998), laser angioplasty (van Leeuwen *et al.* 1993; Vogel *et al.* 1996*b*), myocardial laser revascularization (Klein, Schulte & Gams 1998; Brinkmann *et al.* 1999), arthroscopic cartilage ablation (Smith 1993; Vogel *et al.* 2002); laser shaving (Optics.Org 2005), and the micromanipulation of individual cells (Venugopalan *et al.* 2002).

An important issue that has only recently received attention is the influence of the mechanical properties of biological tissue on the stress wave and cavitation dynamics following pulsed laser ablation and optical breakdown. Earlier experimental studies mostly attempted to assess the laser-induced effects through model studies in water. Jansen *et al.* (1996), Asshauer *et al.* (1997), and Delacretaz & Walsh (1997) presented first studies on holmium-laser-induced bubble formation in more realistic tissue phantoms. Vogel *et al.* (1999*b*) compared the optical breakdown dynamics in water and real tissue. They observed that the shapes of the acoustic transients produced are very different in both cases. As shown in figure 1, optical breakdown in corneal tissue is accompanied by a strong tensile stress wave which is absent in water. Moreover, the bubble expansion phase is shortened to a few microseconds (Vogel *et al.* 1994*b*, 1999*b*), and the stress wave originating from the bubble collapse in water is missing. Since biological tissue is much more susceptible to damage by tensile stress than to compressive stress (Duck 1990), these findings motivated us to investigate the dependence of stress wave generation and cavitation bubble dynamics
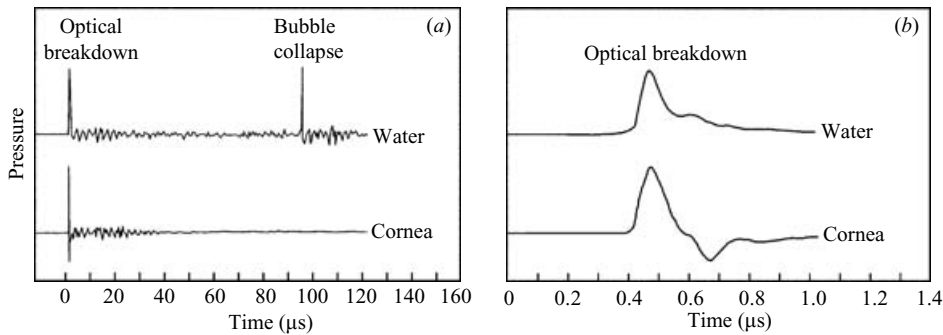
FIGURE 1. Acoustic emission after focusing a 30 ps laser pulse with an energy of 300 μJ in cornea and physiological saline. (*a*) overview of the acoustic signal, (*b*) detailed view of the breakdown pulse. The acoustic signals were measured at 10 mm distance from the breakdown site. The compressive stress amplitude at this distance was 0.24 MPa, the tensile stress amplitude 0.1 MPa.

on the elastic/plastic properties of the medium surrounding the breakdown site in a systematic manner.

The present study describes experimental and numerical investigations of stress wave emission and cavitation bubble dynamics after optical breakdown in a homogeneous elastic tissue phantom with Nd:YAG laser pulses of 6 ns duration. The parameters varied experimentally in this study are the elastic modulus of the medium and the laser pulse energy. The elastic medium consists of a transparent polyacrylamide (PAA) gel whose elastic modulus can be controlled by modifying the water content. The elastic modulus of the PAA samples was varied between 1.7×10^{-2} MPa and 0.4 MPa. This range covers the elastic properties of various biological tissues, such as renal parenchyma (0.06 MPa, Kodama & Tomita 2000), articular cartilage (0.4–1.15 MPa), muscle (0.06–0.8 MPa, Duck 1990), skin (0.13–0.26 MPa measured in suction, Barel, Courage & Clarys 1995; 4–20 MPa measured in tensile testing Manschot & Brakee 1986), and cornea (0.3–0.5 MPa at physiologic conditions, 20–57 MPa for a stress of 0.31 MPa, Hoeltzel *et al.* 1992). A range of E-values is quoted here for each tissue type, because the elastic modulus of biological tissue depends strongly on the applied stress. The laser pulse energy was varied between 0.4 and 12 mJ. These values are typical for clinically used Nd : YAG lasers in intraocular photodisruption (Steinert & Puliafito 1985; Vogel 1997).

We found that the elastic/plastic behaviour of the medium and laser pulse energy strongly influenced both stress wave generation and cavitation bubble dynamics. In a certain parameter range, the stress wave emitted during optical breakdown has a bipolar shape with a leading compressive wave and a trailing tensile wave. The elastic response of the medium leads to a limitation of bubble expansion, a shortening of its oscillation time, and to a reduction of the amplitude of the stress wave emitted during bubble collapse. These changes become ever more pronounced with increasing elastic modulus and plastic yield strength of the medium. For sufficiently stiff media, the bubble oscillation is strongly damped. After reaching the maximum size, the bubble radius oscillates only slightly, and a stress wave originating from bubble collapse is completely absent. The latter case correlates with the generation of strong tensile stress during the initial stages of bubble expansion. The numerical studies revealed that the generation of the tensile stress waves is not correlated to variations of the
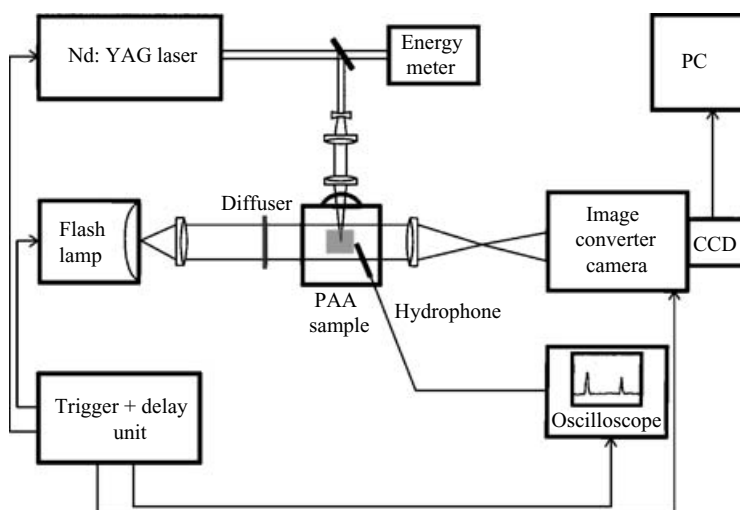
E.-A. Brujan and A. Vogel

FIGURE 2. Experimental arrangement for the investigation of the behaviour of a laser-induced bubble in a tissue phantom (PAA sample).

viscosity of the tissue phantom, but requires a large elastic modulus and a relatively large plastic flow stress of the medium.

The results of our investigations are discussed with respect to collateral damage in short pulsed laser surgery.

2. Experimental methods

2.1. *Bubble generation*

The experimental arrangement for the investigation of the behaviour of laser-induced cavitation bubbles in an elastic medium is depicted in figure 2. The bubbles were generated using a Q-switched Nd:YAG laser (Continuum YG 671-10) which delivers light pulses at 1064 nm wavelength with 6 ns duration and energies of up to 250 mJ. The PAA sample was mounted in a Teflon holder and completely immersed in water during experiments. The laser beam was first expanded by a telescope consisting of a biconcave lens ($f = -40$ mm) and a Nd:YAG laser achromat ($f = 200$ mm), and then focused into a glass cuvette by a second Nd:YAG laser achromat ($f = 125$ mm). This optical arrangement enabled us to use a large focusing angle together with a large distance between laser focus and cuvette walls. A large convergence angle of the laser beam (32° in water) was used to produce compact plasmas and, hence, spherical bubbles. Achromats were used for beam collimation and focusing to minimize spherical aberrations, and for the same purpose an ophthalmic contact lens corrected for an air–water transition (Rodenstock RYM) was built into the cuvette wall (Vogel *et al.* 1996*a, c*). The laser focus coincided with the aplanatic point of the contact lens. Aiming was facilitated by a helium–neon laser beam coupled into the beam path of the Nd:YAG laser. A smooth beam profile and the minimization of aberrations ensured that no 'hot spots' occurred in the focal region of the laser beam and only a single plasma was formed. During each laser exposure, the pulse energy was measured using a pyroelectric energy meter (Laser Precision Rj 7100). The pressure of the stress waves emitted during optical breakdown and first bubble collapse was measured using a PVDF needle hydrophone (Ceram) with a rise time of

Sample	Water	PAA–95% water	PAA–85% water	PAA–80% water	PAA–70% water
E (MPa)	–	0.017 ± 0.001	0.124 ± 0.004	0.3 ± 0.01	0.4 ± 0.01
Y_0 (MPa)	–	–	20	60	80
ρ (kg m^{-3})	998	1012 ± 10	1032 ± 10	1050 ± 10	1073 ± 10
c_0 (m s^{-1})	1483	1518 ± 15	1560 ± 15	1575 ± 15	1605 ± 15

TABLE 1. Values of the elastic modulus E, plastic yield strength at large strain rates Y_0, density ρ, and sound velocity c_0 of the PAA samples at $20\,^{\circ}$C and ambient pressure.

12 ns, an active area of 1 mm^2, and a sensitivity of 21 mV MPa^{-1}. The hydrophone was connected to an oscilloscope with 1 MΩ input impedance to ensure proportionality between voltage and pressure. The hydrophone was placed in water, 10 mm away from the emission centre. Here the portion of the shock wave intersecting the active area of the hydrophone can be approximated by a plane wave, and no distortions of the detected waveform are expected (Vogel *et al.* 1996*a*). The propagation of the acoustic transient from PAA into water will hardly affect its shape and amplitude because both materials have almost the same acoustic impedance $\rho \, c_0$ (see table 1).

2.2. *Tissue phantom*

The tissue phantom consisted of transparent gels of polyacryalmide (PAA) with a water content of 95%, 85%, 80% and 70%, respectively. For 70% water content, 60 g acrylamide and 1.6 g *bis*-acrylamide were mixed with 140 g of 0.22M aqueous Tris buffer (pH 9.5) and 1 ml 10% ammoniumpersulfate (APS). The solution was then placed in a plastic container and mixed with 0.2 ml N,N,N',N'-tetramethyl-ethylenediamine (TEMED) to initiate polymerization. For higher water content, the stock solution was diluted with buffer. A plastic grid was placed in the container to enable simultaneous production of 49 PAA samples, each having a volume of $20 \times 15 \times 15$ mm^3. The large number of samples produced in each batch ensured reproducible conditions throughout the measurement series. All components for the PAA-preparation were obtained from BioRad Laboratories. To avoid perturbations of the bubble dynamics caused by remaining deformations of the PAA sample, a new sample was used for every laser exposure. We preferred PAA to other tissue phantoms such as gelatin or agar because of its high melting point above the water boiling point.

The elastic properties of the PAA samples were quantified by determining the stress–strain relation and calculating the elastic modulus, E, as the slope of the stress–strain curve. Uniaxial compression tests were performed on three specimens of PAA samples at each water content using a universal testing machine (Zwick 1456). The elastic modulus of the PAA samples was determined at 10% strain, with a standard deviation in E smaller than 7%.

For PAA with 80% water concentration, we determined the complete stress–strain curve both under uniaxial compressive and tensile load up to mechanical failure (figure 3). A constant deformation rate of 1 mm min^{-1} was applied to 10 mm thick specimens. The corresponding strain rate was $\dot{\varepsilon} = 1.7 \times 10^{-3}$ s^{-1}. A strain of up to 60% could be achieved under tensile load before the sample broke. The ultimate tensile strength was $Y = 0.056$ MPa. Under compression, the sample broke at a pressure of $Y = 0.54$ MPa. In both cases, failure probably starts at micro-cracks or other tiny irregularities at the sample surface.
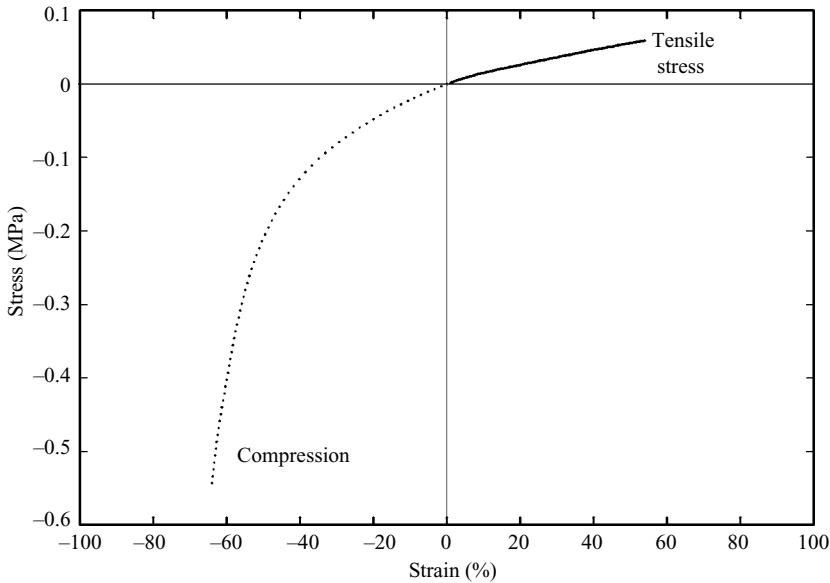
FIGURE 3. Stress-strain curve for PAA with 80% water content under tensile and compressive load. The curves were recorded with a strain rate of $\dot{\varepsilon} = 1.7 \times 10^{-3}\,\mathrm{s^{-1}}$ (a deformation of $1\,\mathrm{mm\,min^{-1}}$ was applied to $10\,\mathrm{mm}$ long specimens) until mechanical failure of the specimen occurred.

It is known that the mechanical properties of polymers depend on the rate of loading (Taylor 1946; Kolsky 1949), and the same is true for biological tissues (Vogel 1972; Haut 1989; Dombi, Haut & Sullivan 1993; Vogel & Venugopalan 2003; Fung 1993). Unfortunately, we did not have the means to determine the elastic modulus under large strain rates (Nicholas & Rajendran 1990). However, we can estimate the plastic yield strength of the samples at large strain rates using results from previous investigations of high-speed liquid jet impact on PAA samples (Brujan et al. 2001a, b). Jets were generated during the collapse of a cavitation bubble near the PAA sample and observed by high-speed photography. Jet impact velocities vary, depending on the relative distance between bubble and PAA sample. The plastic yield strength is estimated by calculating the impact pressure generated by a jet that is just capable of penetrating the PAA sample. The water hammer pressure of a jet with a flat tip is (Brunton 1966)

$$p_{\mathrm{WH}} = \frac{\rho_1 c_1 \; \rho_2 c_2 \; v}{\rho_1 c_1 + \rho_2 c_2}, \qquad (2.1)$$

where ρ_1, c_1 and ρ_2, c_2 are the respective densities and sound velocities in the jet and the impacted material, and v is the jet velocity. The water hammer pressure lasts for a time $t_{\mathrm{WH}} = r_{\mathrm{jet}}/c_1$ during which the relaxation wave travels from the periphery into the centre of the jet. This time is of the order of 10–20 ns (Brujan et al. 2001b). The adopted value of the yield strength of the material corresponds to the lowest jet velocity for which a penetration into the PAA sample was observed. It should be noted here that this is only a low estimate of the yield strength of the material since the impact pressure can be up to three times higher than the value given by equation (2.1) when the jet tip is round or conical (Lesser & Field 1983). The measured values of the elastic modulus, density and sound velocity, as well as an estimation of the yield strength of the PAA samples are summarized in table 1.

The values in table 1 for the plastic yield strength determined at very large strain rates are much larger than the value for the ultimate tensile strength that was obtained at a slow deformation rate (60 MPa *vs.* 0.056 to 0.54 MPa for the PAA sample with 80% water content). For tissues, it is also known that the ultimate tensile strength increases with strain rate (Vogel 1972; Haut 1989; Dombi *et al.* 1993; Vogel & Venugopalan 2003). It is likely that a similar dependence on strain rate also applies for the elastic modulus. Up to a 10-fold increase of the elastic modulus compared to quasi-static values was observed in impact experiments on polymers with a Hopkinson pressure bar (Kolsky 1949) with which strain rates of the order of $\dot{\varepsilon} = 10^3\,\mathrm{s}^{-1}$ can be reached, and a strain rate dependence of the elastic modulus has also been reported for biological tissues (Fung 1993, chap. 7.8) These results indicate that the effective E-values during the initial phase of the cavitation bubble dynamics where strain rates of the order of $10^6\,\mathrm{s}^{-1}$ are reached may be considerably larger than those given in table 1.

It should be noted that the ultimate tensile strength of many soft biological tissues is about one order of magnitude larger than that measured for PAA, even though the elastic modulus is quite similar (Duck 1990). Furthermore, tissue usually becomes stiffer with increasing tensile load (Yamada 1970) whereas PAA, like most polymers, becomes more compliant.

2.3. *High-speed photography*

The dynamics of the cavitation bubble was recorded with a high-speed image converter camera (Hadland Photonics, Imacon 792). A framing rate of 50 000 frames s^{-1} was chosen for the overview series of the bubble motion at $\times 1.5$ original magnification. The image on the fluorescent screen of the image converter camera was recorded with a cooled slow scan CCD camera system (Photometrics AT200A) with a 1317×1035 pixel array. The signal of the CCD camera was then digitized with 8-bit resolution (128 grey levels) and passed to a computer. The recorded images show a spatial resolution in object space of 58 μm. The devices were triggered electronically with controlled delay times for taking specific sequences out of the overall bubble motion.

2.4. *Bubble energy and bubble oscillation time*

Both energy and oscillation time of a spherical bubble situated in a liquid medium of infinite extent are related to its maximum radius $R_{\max}$. The potential energy is given by

$$E_B = \tfrac{4}{3}\pi(p_0 - p_v)R_{\max}^3, \tag{2.2}$$

where p_0 is the static pressure, and p_v the vapour pressure of the liquid. The oscillation time T_{osc} is (Rayleigh 1917):

$$T_{osc} = 1.83\left(\frac{\rho_0}{p_0 - p_v}\right)^{1/2} R_{\max}, \tag{2.3}$$

where ρ_0 is the density of the medium. Tomita & Shima (1990) confirmed both equations for bubbles oscillating in water in experiments performed with maximum bubble radii of between 0.06 mm and 1.8 mm.

When a bubble is generated in an elastic/plastic medium, part of the energy going into bubble expansion is required to overcome the elastic restoring forces and viscous damping. Therefore, the expanded bubble is smaller, and for calculating its potential energy, we must add a pressure term representing the elastic forces of the medium (Glinsky *et al.* 2001). The smaller bubble sizes coincide with shorter oscillation times.

Moreover, the damping of the bubble oscillation distorts the symmetry between expansion and collapse phase, so that equation (2.3) no longer holds. In the case of a strongly damped oscillation, T_{osc} is much larger than predicted by equation (2.3).

In our experiments, we compared the bubble oscillation times in PAA samples of different water content with the oscillation time in water at equal laser energy to assess the influence of the elastic/plastic medium. The oscillation periods were obtained by measuring the time interval between the shock waves emitted during optical breakdown and first bubble collapse.

3. Numerical methods

We used a spherical model of bubble dynamics valid to first-order in the bubble-wall Mach number (Lezzi & Posperetti 1987). This model assumes a constant gas content of the bubble, neglecting gas diffusion through the bubble wall and heat conduction. We also assume that vapour is not present in the bubble. We make this assumption to avoid the complications caused by evaporation and condensation at the bubble interface. The bubble dynamics is described by the equation:

$$R\ddot{R} + \tfrac{3}{2}\dot{R}^2 - \frac{1}{c_0}(R^2\dddot{R} + 6R\dot{R}\ddot{R} + 2\dot{R}^3) = H, \qquad (3.1)$$

where R is the time-dependent bubble radius, dots denote a time derivative, c_0 is the undisturbed speed of sound in the medium, and H is the enthalpy change between bubble wall and infinity,

$$H = \frac{n(p_0 + B)}{(n-1)\rho_0}\left[\left(\frac{P+B}{p_0+B}\right)^{(n-1)/n} - 1\right]. \qquad (3.2)$$

The constants B and n relate to the Tait equation of state for water that was used to derive equation (3.2). The pressure P at the bubble interface is

$$P = \left(p_0 + \frac{2\sigma}{R_n}\right)\left(\frac{R_n}{R}\right)^{3\kappa} - \frac{2\sigma}{R} - 4\eta\frac{\dot{R}}{R} - F[R(t)]. \qquad (3.3)$$

Here, R_n denotes the equilibrium radius of the bubble, κ the ratio of the specific heat at constant pressure and volume, σ the surface tension, η the medium viscosity, and F the radial deviatoric stress corresponding to the elastic/plastic properties of the medium.

The equation describing the pressure distribution in the medium surrounding the bubble is:

$$\frac{p(r)}{p_0} = 1 + \frac{(R^2\ddot{R} + 2R\dot{R}^2)(\tau)}{r} - \frac{1}{c_0}\frac{R}{r}(R^2\dddot{R} + 6R\dot{R}\ddot{R} + 2\dot{R}^3)(\tau) - \frac{(R^2\dot{R})}{2r^4}, \qquad (3.4)$$

where $\tau = t - (r-R)/c_0$ and, unless indicated, all the R have the argument t.

In obtaining equations (3.3) and (3.4) we used the facts that, for a linear viscoelastic medium, the incompressible formulation is valid close to the bubble wall ($r \sim R$) while the far field is governed by linear acoustics (Brujan 1999). The far-field condition is defined by $r \sim cT$, with c being the speed of sound in the liquid and T a characteristic time such as the collapse time. The last two terms in equation (3.3) determine the viscous and elastic/plastic response of the medium. The form of the first damping term is obtained by assuming that processes of internal friction occur when different material 'particles' move relative to each other. To obtain the second damping term
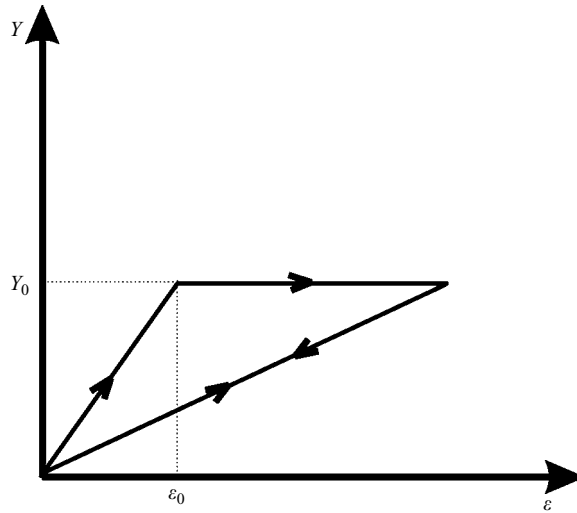
FIGURE 4. Stress–strain behaviour assumed for the numerical simulations. The relation between elastic modulus E and shear modulus G corresponding to the linear part of the stress–strain curve is $E \cong 3G$.

we have considered an isotropic elastic/plastic material behaviour with a constant yield surface. Figure 4 shows the stress–strain relationship assumed for our numerical simulations. The medium is assumed to be locally linearly elastic with a shear modulus G and plastic flow stress Y_0. This assumption is a strong simplification of real dynamic stress-strain curves for polymers such as presented by Taylor (1946). The shear modulus is related to the elastic modulus E by $E = 2(1 + \mu)G$ where $\mu \approx 0.5$ is the ratio between lateral contraction and axial strain. We therefore obtain $G \approx E/3$. When the plastic flow stress is reached, the material fails at a radius R_d so that the stress remains clamped at Y_0. For stress values below Y_0 the medium reacts elastically again. This gives the expression (Glinsky *et al.* 2001)

$$F = 4G \left(\frac{R - R_0}{R_0} \right) \left(\frac{R^2 + R_0 R + R_0^2}{3R_d^3} \right) \tag{3.5}$$

for the radial deviatoric stress, where R_0 is the initial radius of the bubble, and R_d is the radius at which the material failed. The radius R_d is related to the failure strain $\varepsilon_0 = Y_0/2G$ by

$$R_d = \left(\frac{2 \left| R_f^3 - R_0^3 \right|}{3\varepsilon_0} \right)^{2/3}, \tag{3.6}$$

where R_f is the maximum bubble radius reached up to the failure time t. Possible changes in the shear modulus arising from material failure around the expanding cavitation bubble (Glinsky *et al.* 2001) are not considered.

The only damping mechanisms accounted for explicitly in this model are those due to medium viscoelasticity and compressibility. Other energy dissipation mechanisms such as crack formation in the medium during bubble expansion are not considered, as well as heat conduction, gas diffusion through the bubble wall, and vapour condensation during bubble expansion. Because of the neglect of some damping mechanisms and because real bubbles may deviate from spherical shape, the pressure reached upon bubble collapse is probably overestimated by this spherical model.

Nevertheless, the model enables at least a qualitative comparison to experimental results for elastic/plastic media. Thus it helps to elucidate the dependence of the bubble motion on the conditions encountered in short-pulsed laser surgery.

A striking feature of equation (3.1) is the appearance of the third-order derivative of the bubble radius with respect to time. Its integration thus requires an initial condition for $\dddot{R}$. To the same order of accuracy in the bubble wall Mach number, an initial condition for $\ddot{R}(t)$ can be obtained by substituting the given initial conditions for R and $\dot{R}$ in the incompressible limit ($c_\infty \to \infty$ in equation (3.1)). The calculation then starts with a bubble nucleus that is initially at equilibrium with radius R_0, whereby the volume of this nucleus is identified with the photographically determined plasma size. The deposition of the laser energy is modelled by an increase of the equilibrium radius R_n during the laser pulse, and the laser pulse is modelled by a $\sin^2$ function with half-width τ and total duration 2τ. The temporal development of the equilibrium radius of the bubble during the laser pulse is described by the relation (Vogel *et al.* 1996a):

$$R_n(t) = \left\{ R_{na}^3 + \frac{R_{nb}^3 - R_{na}^3}{2\tau} \left[t - \frac{\tau}{\pi} \sin\left(\frac{\pi}{\tau}t\right) \right] \right\}, \qquad (3.7)$$

where $R_{na} = R_0$. The value of R_{nb} is adopted such that the calculations for water yield the same maximum cavitation bubble size R_{max} as determined experimentally. For PAA, we use the same R_0 and R_{nb} values as for water.

The above bubble dynamics model contains too many parameters to vary all of them in a numerical parameter study. Therefore, we systematically investigate only the influence of those three parameters that have the largest influence on bubble dynamics and stress wave emission: viscosity; elastic modulus; and plastic flow stress. The variation of these parameters allows us to elucidate the origin of the bipolar stress waves after breakdown in tissues, as discussed in §5.2. The influence of surface tension is small unless values three orders of magnitude larger than those for water are used, which is physically unrealistic. Exact values of the nonlinearity parameters B and n for PAA and their dependence on the water content of PAA are not known. However, it seems reasonable to assume that they will resemble the constants valid for water. The largest uncertainty in the modelling is related to the simplifying assumption made for the stress–strain relationship (figure 4). However, more refined relationships cannot be treated in the framework of an analytic model, but require the use of an elaborate hydrodynamic code.

4. Results

4.1. *Experiments*

Figures 5 and 6 show two collections of high-speed photographic records of the bubble dynamics and the corresponding hydrophone signals for values of the laser pulse energy $E_L \approx 1\,\text{mJ}$ and $E_L \approx 10\,\text{mJ}$, respectively. The hydrophone signals were recorded simultaneously with the documented image series. The laser light is incident from below. The rapidly expanding plasma formed during optical breakdown gives rise to a cavitation bubble that grows to a maximum radius which depends on the laser pulse energy and the properties of the surrounding medium. After expansion, bubbles generated in water collapse down to a minimum size until the compressed gas in the bubble leads to a rebound (figures 5a and 6a). Upon collapse, the bubble dissipates energy, mainly through emission of an acoustic transient. Therefore, it re-expands to a smaller radius than that reached after plasma formation. An oscillation
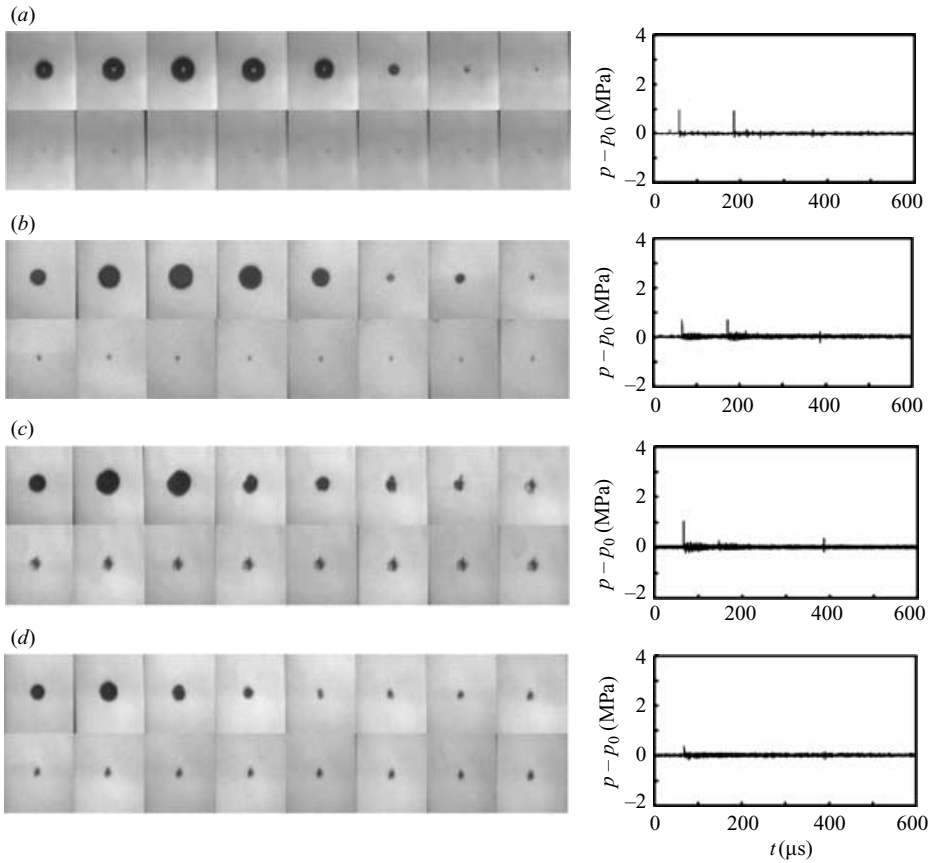
FIGURE 5. Cavitation bubble dynamics in water and PAA samples with different water content c (left-hand column), and the corresponding pressure signal measured at a distance of 10 mm from the laser focus (right-hand column). The laser pulse energy was about 1 mJ. (*a*) water, $E_L = 0.93$ mJ; (*b*) $c = 95\%$, $E_L = 1.36$ mJ; (*c*) $c = 80\%$, $E_L = 1.24$ mJ; (*d*) $c = 70\%$, $E_L = 1.05$ mJ. The first frame was taken 15 μs after the moment of optical breakdown, and the frame interval is 20 μs. Frame width 4 mm.

behaviour similar to that in water is in the PAA samples only observed for large laser pulse energies. With increasing PAA content of the samples, both maximum size and oscillation period of the bubble decrease. For $E_L \approx 1$ mJ and a PAA sample with 70% water content (figure 5*d*), the bubble dynamics is characterized by a strongly damped behaviour where no pronounced collapse and rebound are observed after bubble expansion. The damping is here more strongly related to energy dissipation by the plastic deformation of the PAA sample and the crack formation in the vicinity of the bubble than to acoustic transient emission. Both damping mechanisms become more important as the crosslinked PAA content of the phantom increases.

For all experimental conditions, the largest pressure transient is produced during optical breakdown. This transient is followed by a weaker pressure transient associated with the first bubble collapse. In the case of water, the second transient is almost as high as the first one, and for $E_L = 10$ mJ it is followed by a third pressure transient generated during the second bubble collapse. In contrast, for the PAA sample with 70% water content, the pressure signal is characterized by the absence of a transient
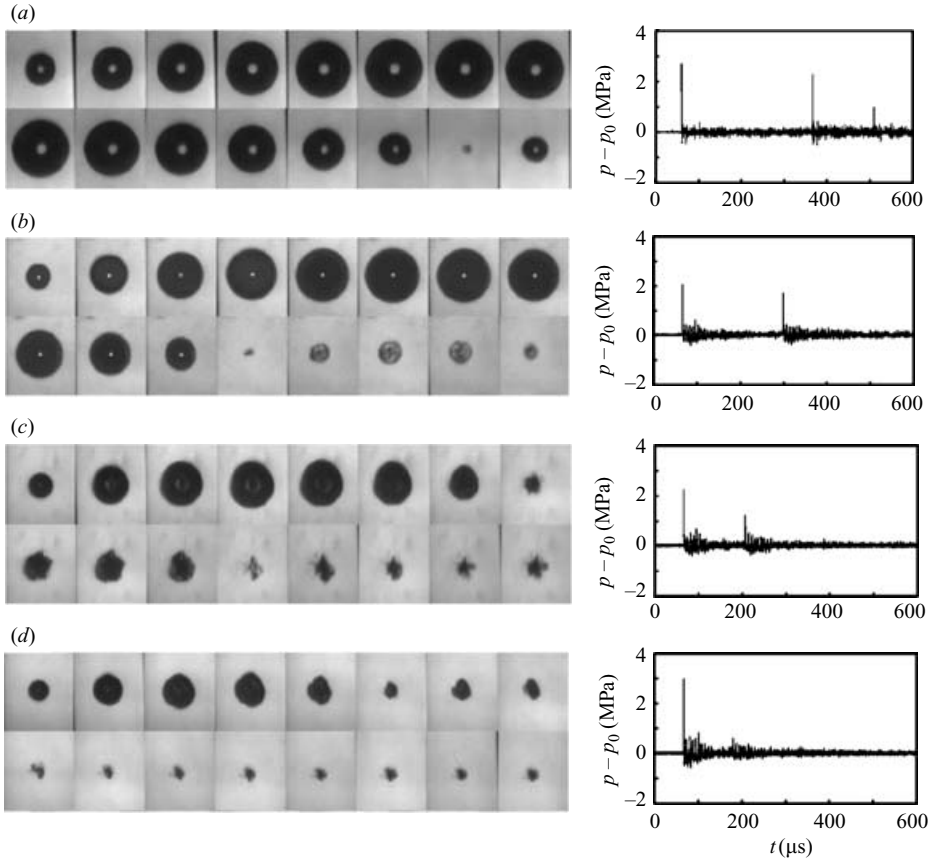
FIGURE 6. Cavitation bubble dynamics in water and PAA samples with different water content c (left-hand column), and the corresponding pressure signal measured at a distance of 10 mm from the laser focus (right-hand column). The laser pulse energy was about 10 mJ. (*a*) water, $E_L = 10$ mJ; (*b*) $c = 95\%$, $E_L = 9.8$ mJ; (*c*) $c = 80\%$, $E_L = 8.2$ mJ; (*d*) $c = 70\%$, $E_L = 10.12$ mJ. The first frame was taken 15 μs after the moment of optical breakdown, and the frame interval is 20 μs. Frame width 4 mm.

emitted during bubble collapse when $E_L \approx 1$ mJ. This is a consequence of strong damping of the bubble oscillation. The collapse occurs earlier in stiffer PAA samples with lower water content since here the bubble is smaller.

The maximum pressure amplitude of the breakdown stress wave is plotted in figure 7 as a function of laser pulse energy. The pressure values refer to a distance r of 10 mm between the laser focus and the measurement site. In this and all following figures, each data point represents the average of six measurement values. At a given laser pulse energy, the stress wave amplitude is quite similar for water and the PAA samples. As expected, the amplitude increases with increasing laser pulse energy E_L. For example, the maximum shock wave pressure in water is 0.7 MPa for $E_L = 1$ mJ and 2.64 MPa for $E_L = 10$ mJ. Both values are in good agreement with the results presented by Vogel *et al.* (1996*a*). The maximum pressure amplitude of the shock waves is approximately proportional to $E_L^{1/2}$ for all types of samples and energy values well above the optical breakdown threshold; but for $E_L < 1$ mJ, the energy
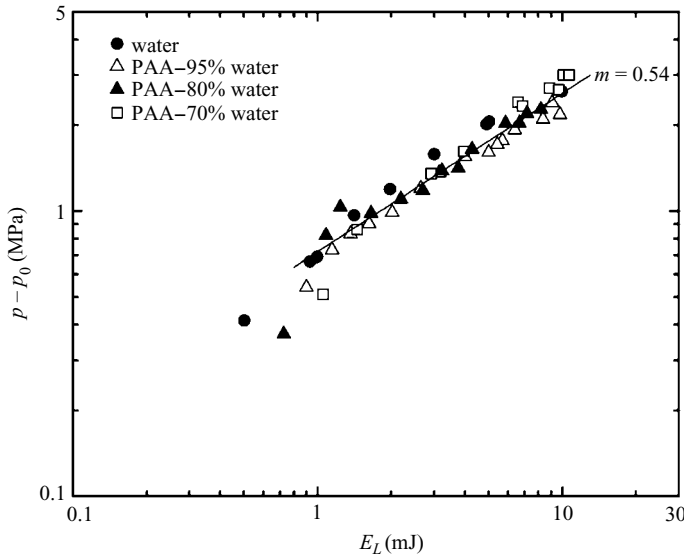
FIGURE 7. Maximum amplitude of the shock wave emitted during optical breakdown, p, as a function of the laser pulse energy, E_L. The values are measured at a distance of 10 mm from the laser focus. The scaling law between the two parameters is $p \propto E_L^{1/2}$.

dependence is steeper. A proportionality $p \propto E_L^{1/2}$ was also observed by Shoeffman, Schmidt-Kloiber & Reichel (1987) for laser-induced optical breakdown in water.

Temporal profiles of the stress waves emitted during optical breakdown in water and in PAA samples with 80% and 70% water content are shown in figure 8. The laser pulse energy E_L was about 10 mJ in all cases. The stress waves exhibit a shock front with 12 ns rise time, equal to the rise time of the hydrophone. The actual rise time is probably shorter (Vogel *et al.* 1996*a*). By contrast, the duration of the pressure pulse is much longer than the response time of the hydrophone and can thus be considered as real. The signals recorded in water and in PAA with 80% water content show only a compressive wave with ≈ 180 ns duration (FWHM) while for the PAA sample with 70% water content, the compressive wave with 250 ns duration is followed by a tensile wave of lower amplitude and 150 ns duration. The ratio of the peak amplitudes of the compressive and tensile waves is 7.5:1. A bipolar shape of the stress wave emitted during optical breakdown was observed only for PAA samples with 70% water content and laser pulse energies of 10 mJ or larger. For all other samples and for smaller values of E_L, the stress transient consisted only of a compressive wave. A bipolar shape of the initial stress transient is, hence, correlated with a large elastic modulus of the medium. The pressure oscillations at later times visible in the recordings for the PAA samples in figures 5 and 6 have a much longer period than the initial stress transient and are probably related to vibrations within the entire PAA sample caused by the propagation and reflection of the initial transient.

Figure 9 presents the maximal bubble radius as a function of the laser pulse energy. At equal laser pulse energy, the maximum radius of the cavitation bubble decreases with decreasing water content of the sample, i.e. with increasing elastic modulus. The scaling law for the bubble size in the PAA samples is the same as that for water, namely, the maximum bubble radius is proportional to the cube root of the laser pulse energy. This scaling law applies, however, only to laser pulse energies larger than 2 mJ,
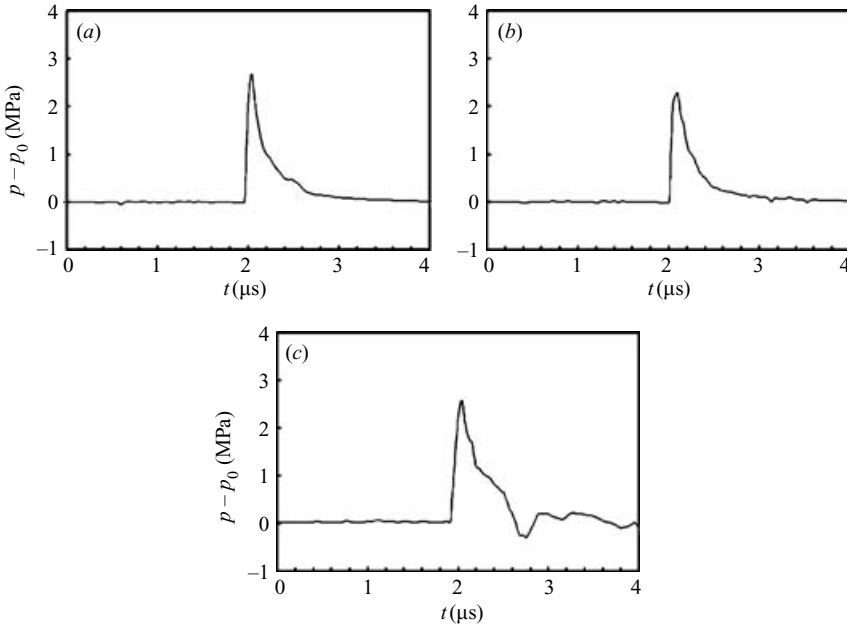
FIGURE 8. Temporal profile of the shock wave emitted during optical breakdown in water (*a*) and in PAA samples with (*b*) 80% water content, and (*c*) 70% water content. The laser pulse energies E_L were 10.0 mJ in (*a*), 8.2 mJ in (*b*), and 10.1 mJ in (*c*). A monopolar pressure pulse is observed in water and in PAA with 80% water content, while a bipolar pressure pulse is observed in the stiffer PAA sample with 70% water content. The peak amplitude of the tensile stress component in (*c*) (0.35 MPa) amounts to 13.7% of the peak amplitude of the compressive stress (2.55 MPa).
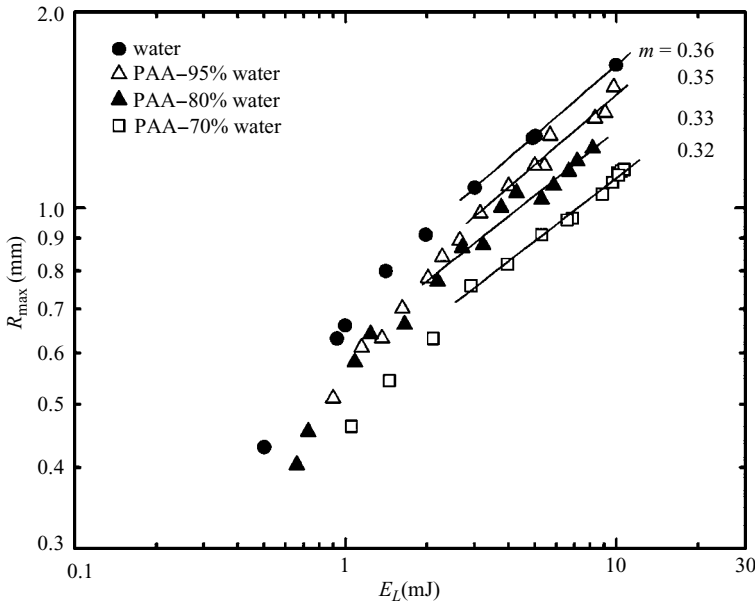
FIGURE 9. Maximal cavitation bubble radius, R_{max}, as a function of the laser pulse energy, E_L. The slope of the straight lines gives the scaling law for the bubble radius at energy values well above the breakdown threshold. The same scaling law applies in water and PAA samples: $R_{max} \propto E_L^{1/3}$.
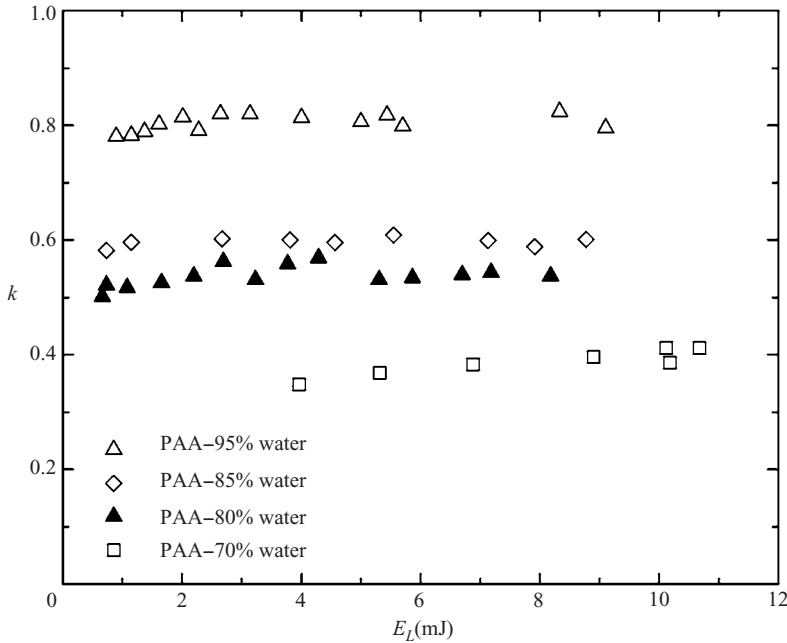
FIGURE 10. Values of the shortening factor k of the oscillation period of a bubble generated inside PAA samples of different water content, plotted as a function of the laser pulse energy.

well above the breakdown threshold. Closer to the threshold, the energy dependence of the bubble size is stronger, similar to that of the initial pressure amplitude. A proportionality $R_{\max} \propto E_L^{1/3}$ was also found by Vogel *et al.* (1994*a*) for laser-induced cavitation bubbles in water.

The diminution of the bubble radius in PAA is coupled with a shortening of the bubble oscillation time. To compare the bubble oscillation times in PAA and water, we define a shortening factor $k = T_{\mathrm{osc,PAA}}/T_{\mathrm{osc,water}}$. Figure 10 shows this factor k as a function of laser pulse energy for all investigated samples. It is almost independent of the laser pulse energy. The bubble oscillation time is always smaller in PAA than in water and decreases with smaller water content, i.e. with increasing stiffness. For the sample with 70% water content, the oscillation time amounted, on average, to only 39% of that in water.

Figure 11 shows the potential energy E_B of the cavitation bubbles according to equation (2.2) plotted as a function of the laser pulse energy. We find that E_B increases proportionally to E_L. The graph suggests, furthermore, that the amount of laser light energy transformed into bubble energy decreases with the water content of the sample. In water, about 20% of the laser pulse energy is converted into bubble energy, whereas the conversion efficiency seems to decrease to about 6% in the PAA sample with 70% water content. However, since the elastic restoring forces in the PAA medium can be expressed as an increase of the pressure at the bubble wall (equations (3.3) and (3.5)), the actual potential energy of the bubble is larger than the value given by equation (2.2) in which only the hydrostatic pressure is considered. It will be between the value for water and the value suggested by figure 11. The remaining part of the bubble energy is dissipated by viscous damping and crack formation.

The damping of the bubble oscillation in PAA results in a reduction of the amplitude of the stress transient emitted upon bubble collapse, and the irregularities
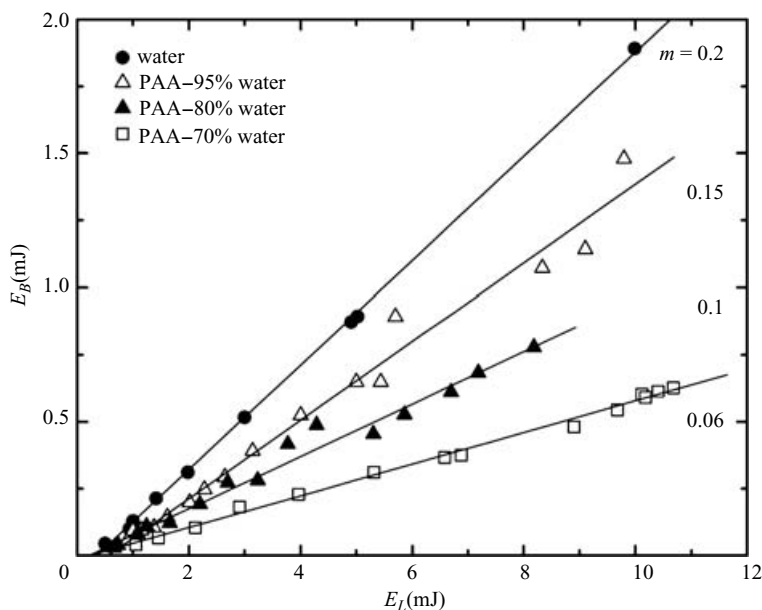
FIGURE 11. Cavitation bubble energy, E_B, as a function of the laser pulse energy, E_L. The slope of the straight lines gives the efficiency by which light energy is converted into bubble energy (equation (2.1)). It is 20% for water, 15% for the PAA sample with 95% water content, 10% for the PAA sample with 80% water content, and 6% for the PAA sample with 70% water content.

associated with crack formation during the bubble oscillations lead to a broadening of the temporal profile of the shock wave emitted during the collapse. The amplitude reduction is shown in figure 12 where the amplitude of the transient emitted during the first bubble collapse is plotted as a function of the laser pulse energy. For water and the PAA sample with 95% water content, the measured values are fitted by a curve $(p_c - p_0) = a E_L^b$, with $a = 1$ and $b = 0.38$ for water, and $a = 0.73$ and $b = 0.4$ for the PAA sample with 95% water content. For the PAA sample with 80% water content, the energy dependence is quite different. Here, the measured values are fitted by a curve $(p_c - p_0) = a(E_L - E_{L,c})^b$, with $a = 0.61$, $b = 0.34$, and $E_{L,c} = 1.01$ mJ. The fit parameter $E_{L,c}$ can be interpreted as a critical value of the laser pulse energy which determines the behaviour of the bubble: strongly damped behaviour occurs if $E_L \leqslant E_{L,c}$, and damped oscillatory behaviour if $E_L > E_{L,c}$. For the PAA sample with 70% water content, the value of $E_{L,c}$ is larger, it is between 8.90 mJ, where no pressure pulse was generated during bubble collapse, and 10.12 mJ where the first transient was observed.

4.2. *Numerical calculations*

We shall now examine the results of the numerical simulations to ascertain some of the effects that the mechanical properties of the medium can have on the bubble dynamics and to explain the origin of the experimental findings reported above. To be able to distinguish the separate phenomena caused by viscosity, elasticity and yield strength of the medium, we vary just one of these properties in any single calculation. We examine the effects of the different mechanical properties on the evolution of the bubble radius, pressure at the bubble wall, and temporal profile of the pressure wave
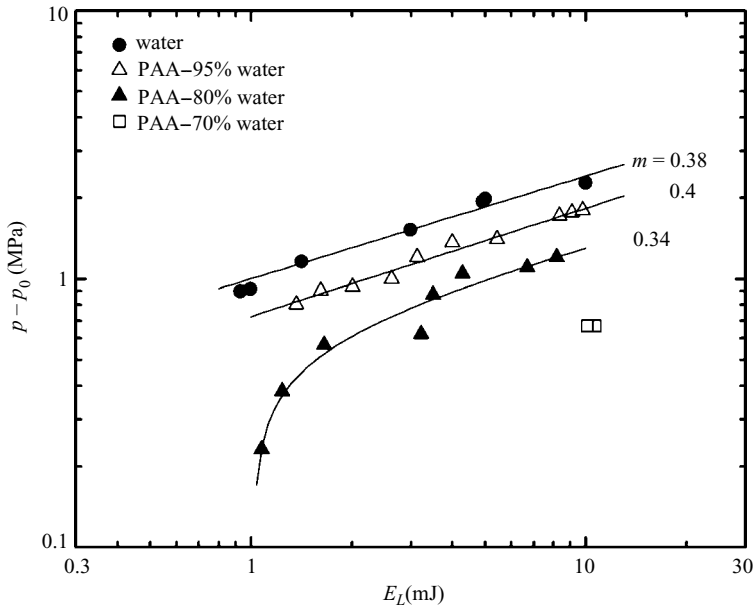
FIGURE 12. Maximum amplitude of the shock wave emitted during first bubble collapse as a function of the laser pulse energy. The values are measured at a distance of 10 mm from the laser focus. For energies well above the threshold the scaling law between maximum shock wave pressure during first bubble collapse and laser pulse energy is $p_c \propto E_L^{1/3}$. For PAA samples with 80% and 70% water content, a critical value of E_L exists below which no pressure pulse is generated during the first bubble collapse (see also text).

emitted during optical breakdown. Particular emphasis will be laid on elucidating the remarkable finding of bipolar stress waves after optical breakdown in tissues.

In light of the potential medical applications related to this work, the values of the elastic modulus, yield strength and viscosity are chosen to cover the range found in biological tissues (Duck 1990). For all calculations it is assumed that the interior gas is air, such that $\kappa = 1.4$, and that the medium surrounding the bubble has the surface tension and density of water ($\sigma = 0.0725\,\mathrm{N\,m^{-1}}$, and $\rho = 999.8\,\mathrm{kg\,m^{-3}}$, respectively). Other pertinent numerical values of the constants in equations (3.1) to (3.7) are $n = 7.15$, $B = 305\,\mathrm{MPa}$ and $p_0 = 0.1\,\mathrm{MPa}$. The values of the initial parameters adopted in the calculations are $R_{na} = 37\,\mu\mathrm{m}$ and $R_{nb} = 642\,\mu\mathrm{m}$ and correspond to the case of bubbles generated in water at a laser pulse energy of 10 mJ (Vogel *et al.* 1996a). Actual values for biological tissue may differ, but their exact values have not yet been determined. To enable comparison with experimental data, all stress amplitudes are calculated for a distance of 10 mm from the bubble centre, and the $p(r)$ results obtained using equation (3.4) are translated in $p(t)$ curves by considering the value of the normal sound velocity in water.

Figure 13 (*a–c*) shows the effect of medium viscosity on the radius time curve of the bubble, pressure at the bubble wall, and on the temporal profile of the stress wave emitted during optical breakdown. In the case of water, good agreement is found between calculated and experimental results. For example, the calculated values of the amplitude and width (FWHM) of the pressure pulse emitted during optical breakdown are 3.1 MPa and 220 ns, respectively. The corresponding experimental values are 2.7 MPa and 180 ns, respectively (figures 7 and 8). The agreement is not
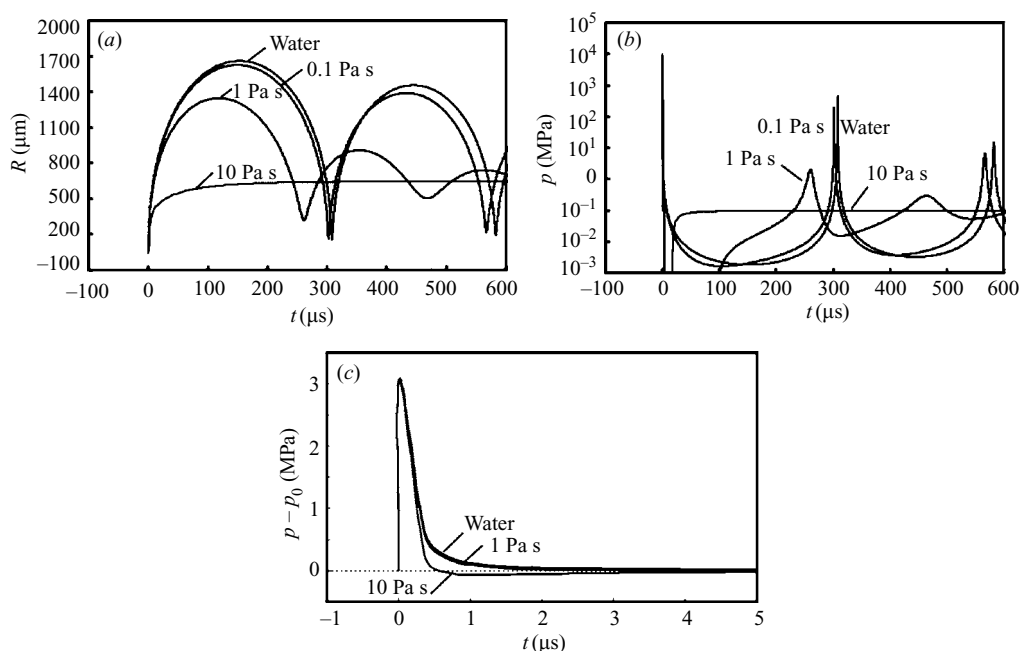
FIGURE 13. Numerical simulations of the influence of medium viscosity on the variation with time of the bubble radius (a), maximum pressure at the bubble wall (b), and temporal profile of the shock wave emitted during breakdown (c) for $E_L = 10$ mJ and $G = E = 0$. The initial parameters used in the calculations were $R_{na} = 37\,\mu$m and $R_{nb} = 642\,\mu$m.

as good for the collapse stress wave, where the calculated pressure amplitude is relatively low. This is probably a consequence of the assumption of a constant gas or vapour content ($R_{nb} = $ const.) throughout the entire bubble oscillation. Ebeling (1974) showed that the equilibrium bubble radius has to be reduced for the calculation of the collapse phase to account for the fact that vapour produced during breakdown condenses during the bubble oscillation. The reduced gas content leads to a stronger emission of acoustic energy during the bubble collapse, i.e. to a larger amplitude of the emitted stress wave. Moreover, the bubble size after rebound is smaller because more energy has been carried away by the collapse wave. The effect of medium viscosity is to decrease the maximal radius and the oscillation period of the bubble (figure 13a). A strongly damped behaviour of the bubble is observed for $\eta = 10$ Pa s. In this case, no collapse wave is emitted, and the pressure at the bubble wall quickly approaches the static pressure in the liquid, p_0 (figure 13b). The temporal profile of the pressure pulse emitted during optical breakdown consists for $\eta < 1$ Pa s only of a compressive wave. For $\eta = 10$ Pa s, the compressive wave is followed by a weak tensile stress wave with a peak amplitude of -0.07 MPa and a duration of several microseconds (figure 13c).

The effect of medium elasticity on the bubble dynamics is similar to that of viscosity: the bubble oscillation is damped and the amplitude of the pressure pulse during collapse is smaller than in the case of water (figure 14a, b). Only a minor difference was found for the peak amplitudes of the compressive stress wave produced during optical breakdown. In water, the maximum value of the bubble wall pressure is 8790 MPa, and for $G = 50$ MPa (corresponding to $E \approx 150$ MPa) it is only 1.6% lower. Therefore, it is not possible to distinguish both traces in figure 14(b). The dominant
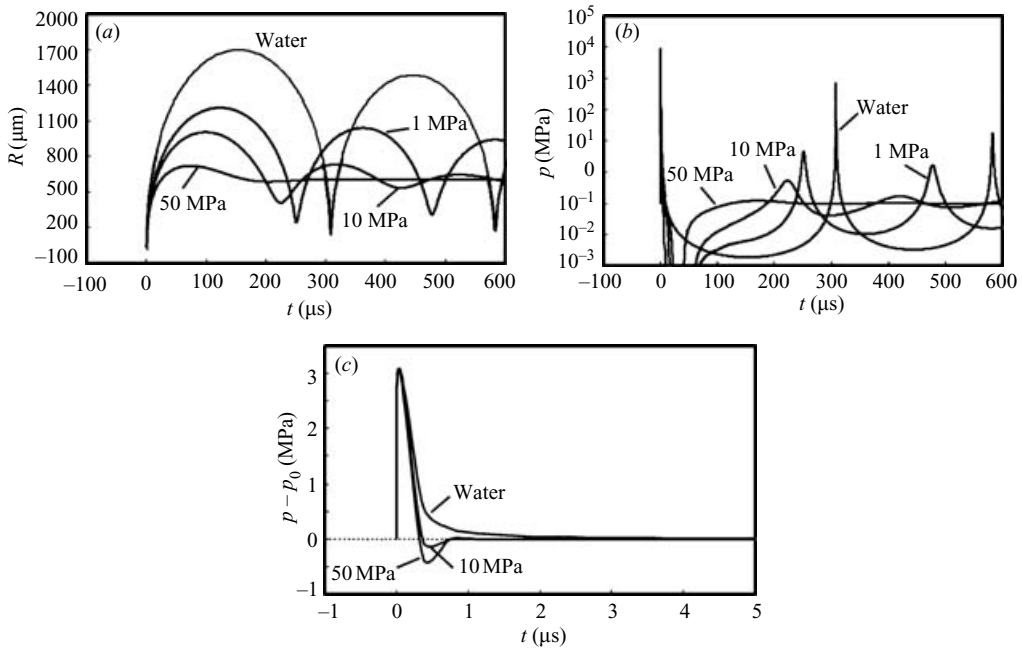
FIGURE 14. Numerical simulations of the influence of medium elasticity on the variation with time of the bubble radius (*a*), maximum pressure at the bubble wall (*b*), and temporal profile of the shock wave emitted during breakdown (*c*) for $E_L = 10$ mJ, $Y_0 = 10^2$ MPa and $\eta = 10^{-3}$ Pa s. The initial parameters used in the calculations were $R_{na} = 37$ μm and $R_{nb} = 642$ μm.

feature of stress generation upon breakdown in elastic media is the generation of a pronounced tensile stress wave following the compressive peak (figure 14*c*). The ratio of tensile and compressive wave amplitudes increases with the medium elasticity and amounts to 1:7 for $G = 50$ MPa, corresponding to a peak negative pressure of -0.44 MPa.

The effect of plastic flow stress on the bubble dynamics is summarized in figure 15 for $G = 50$ MPa and $\eta = 10^{-3}$ Pa s. A large plastic flow stress of the medium leads to a small bubble radius and a small amplitude of the collapse stress wave. For stress values above the plastic flow stress Y_0, the material acts like a liquid. With decreasing Y_0, the damping effect of medium elasticity is manifested for a shorter period of time. Therefore, the $R(t)$ and $p(t)$ dynamics approach that of water when Y_0 is diminished. Specifically, the tensile stress transient after breakdown vanishes for small plastic flow stresses.

Figure 16 illustrates the temporal profile of the stress wave emitted during optical breakdown for large values of the medium elasticity similar to those of human hair (Duck 1990), which is of interest in the context of laser shaving mediated by optical breakdown (Optics.Org 2005). The values of the plastic flow stress and medium viscosity adopted in the calculations are $Y_0 = 200$ MPa and $\eta = 10^{-3}$ Pa s. The calculations predict a reduction of the peak compressive stress and an increase of tensile stress with increasing medium elasticity. At $G = 9000$ MPa the reduction of the compressive stress compared to the traces in figure 14 is not significant, but it becomes considerable at $G = 30000$ MPa where it drops to -2.49 MPa. For this G value, the compressive wave is followed by a strong tensile wave with a peak amplitude of -1.73 MPa, which amounts
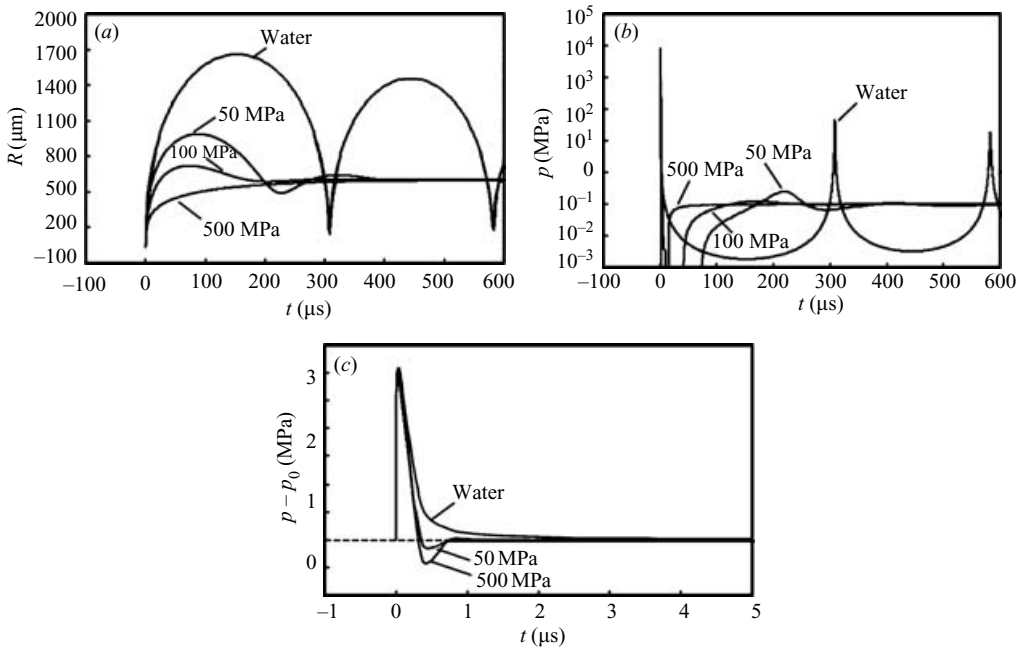
FIGURE 15. Numerical simulations of the influence of plastic flow stress on the variation with time of the bubble radius (a), maximum pressure at the bubble wall (b), and temporal profile of the shock wave emitted during breakdown (c) for $E_L = 10$ mJ, $G = 50$ MPa (corresponding to $E \approx 150$ MPa), and $\eta = 10^{-3}$ Pa s. The initial parameters used in the calculations were $R_{na} = 37\,\mu$m and $R_{nb} = 642\,\mu$m.

FIGURE 16. Numerical simulations of the influence of large values of medium elasticity on the temporal profile of the shock wave emitted during breakdown for $E_L = 10$ mJ, $Y_0 = 200$ MPa, and $\eta = 10^{-3}$ Pa s. The initial parameters used in the calculations were $R_{na} = 37\,\mu$m and $R_{nb} = 642\,\mu$m.

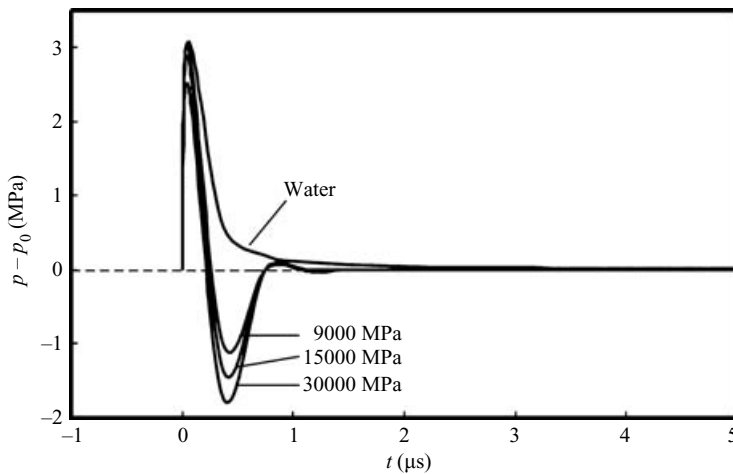to 69.5% of the peak compressive stress amplitude. When the plastic flow stress is raised from 200 MPa to 1000 MPa (not shown), the compressive amplitude remains constant, but the tensile stress amplitude increases to 78% of the compressive stress.

5. Discussion

5.1. *Parameter dependence of stress amplitudes and bubble dynamics*

The present study showed that the mechanical properties of tissue-like media strongly influence the dynamics of laser-produced cavitation bubbles as well as the amplitude and shape of the stress transients emitted during optical breakdown and bubble collapse. The amplitude of the compressive stress transient emitted upon breakdown was very similar for water and all PAA samples, and it did not change when viscosity, elastic modulus and plastic flow stress were varied in the numerical calculations. It simply depends on the size and energy density of the plasma produced during optical breakdown (Vogel *et al.* 1996*a*). However, during the subsequent plasma expansion, the mechanical properties of the medium come into play. They affect the trailing edge of the first stress transient, the bubble oscillation, and the stress wave emission upon bubble collapse. An increase of both medium viscosity and elastic modulus leads to a damping and shortening of the bubble oscillation, a decrease of the stress amplitude produced during bubble collapse, and to the formation of a tensile stress component at the end of the breakdown stress wave. However, the amplitude of the tensile component is much larger in an elastic material than in a predominantly viscous medium.

Our numerical results are, for similar values of the elastic modulus and plastic yield strength, in good qualitative agreement with the findings of a previous study with the MESA-two-dimensional hydrodynamic code (Vogel *et al.* 1999*b*). Unfortunately, the stress wave traces in the previous calculations were distorted by strong numerical noise and non-ideal initial conditions. More recent modelling studies presented Rayleigh-type two-dimensional representations of the bubble evolution at a fibre-optic tip (Glinsky *et al.* 2001; Friedman *et al.* 2002) and explored different constitutive laws for the elastic medium (Emelianov *et al.* 2004). However, these publications provided no information on the shape of the laser-induced stress transients.

5.2. *Origin of the tensile stress*

The most interesting feature of the interaction of the laser pulses with biological tissue phantoms is the generation of a bipolar stress wave during breakdown consisting of a compressive wave followed by a tensile wave of lower amplitude. A weak tensile wave may also occur in an inelastic material with high viscosity. By contrast, no tensile wave, but only a rarefaction wave with underpressure, is produced by breakdown in water.

Conservation of momentum requires that the stress transient emitted from a finite volume within an extended medium must contain both compressive and tensile components such that the integral of the stress over time vanishes (Paltauf & Schmidt-Kloiber 1999; Vogel *et al.* 1999*b*; Paltauf & Dyer 2003). Detailed studies of this phenomenon have been performed for the propagation of thermoelastic stress waves originating from spherical and cylindrical absorbers in a gel (Paltauf & Schmidt-Kloiber 1999), the tip of an optical fibre immersed in an absorbing liquid (Frenz *et al.* 1996), and from the heated volume in a solid sample that was irradiated in air (Itzkan *et al.* 1995). However, the phenomenon has previously not been investigated for stress waves originating from optical breakdown in tissue-like media.

For optical breakdown in a liquid, it is known that the compressive stress peak emitted upon plasma formation is followed by a long rarefaction wave such that the integral of the acoustic transient over time vanishes (Vogel *et al.* 1999*b*). As seen in the traces for water in figures 13–15, the pressure in the rarefaction wave approaches zero but cannot become negative because, during the laser pulse, a cavitation bubble is

formed by vaporization of the liquid in the focal volume. By contrast, in a perfectly elastic medium without bubble formation, the thermo-elastic stress wave originating from a three-dimensional heat pole is symmetric, with compressive and tensile components of equal shape and amplitude (Sigrist & Kneubühl 1978). In the case of optical breakdown in a tissue-like medium, an intermediate behaviour resulting in a compressive and weaker tensile component is found (figures 13–15). The compressive pulse depends little on the viscous and elastic properties of the medium, but because of the shortening of the bubble oscillation time, the rarefaction wave observed in water must become a tensile stress wave. Notably, the rarefaction wave with a tensile stress component is not symmetric in time such as the rarefaction wave in water, but exhibits a tensile stress component only in the initial phase of the bubble expansion. A similar intermediate behaviour is observed when voids form under the action of thermoelastic tensile stress: the shape of the compressive pulse remains the same, but the amplitude of the tensile component is attenuated and its duration prolonged (Strauss *et al.* 2002; Leveugle & Zhigilei 2004). However, although the waveforms produced by the thermoelastic response of a cavitating medium and by optical breakdown in a tissue-like medium resemble each other, their origin is different. While under the action of a thermoelastic stress wave, bubble generation is a consequence of the tensile stress, the tensile stress in a tissue-like elastic–plastic medium arises as a consequence of the strong damping of the bubble oscillations.

The tensile stress component is shorter and has a much larger negative amplitude for elastic–plastic media (figures 14 and 16) than for viscous media (figure 13). The reason for this difference is apparently that the $R(t)$ curve starts to deviate faster from the curve for water in an elastic medium than in a medium with only viscous damping. The tensile wave is most pronounced for the material with largest elastic modulus and yield strength. Even though modelling the tissue as a fluid with high viscosity but little elasticity could explain a damping of the bubble oscillations and the lack of a pronounced collapse, the assumed viscosity must be 5000–10 000 times higher than the viscosity of water to restrict the bubble size to experimentally observed values (see figure 13, and Vogel *et al.* 1999*b*). Moreover, the viscous damping yields only a very small tensile component in the breakdown stress wave, in contrast to the experimental findings. The key feature for the tensile stress generation is the *elastic* tissue response. However, if the deformation were perfectly elastic, the bubble would collapse to a very small radius close to the initial plasma size. Consideration of the plastic deformation in the initial phase of the bubble expansion, when the bubble pressure still exceeds the yield strength of the material, is essential to obtain a realistic bubble size at the end of its damped oscillations. These results corroborate the findings of Chapyak & Godwin (1998) and Brujan *et al.* (2001*a*) who showed the importance of the elastic–plastic tissue response for cavitation-enhanced tissue ablation in a liquid environment. They also agree with experimental findings of Asshauer *et al.* (1997) indicating that for PAA the loss modulus which is representative for viscous damping is more than one order of magnitude smaller than the elastic modulus.

5.3. *Comparison between numerical predictions and experimental observations on tensile stress generation*

Characteristic features of optical breakdown in the corneal stroma are a tensile component in the breakdown stress wave (figure 1), and a fast initial expansion followed by slight oscillations of the bubble radius before a constant value is reached after 50–100 μs (Juhasz *et al.* 1994; Vogel *et al.* 1999*b*). This behaviour was reproduced in our model calculations for a shear modulus of 50 MPa (corresponding to $E \approx 150$ MPa), a plastic yield strength of 100 MPa, and a viscosity of 10^{-3} Pa s

(figure 14*a*). Hoeltzel *et al.* (1992) report values between 0.34 MPa and 0.5 MPa for the elastic modulus of cornea at physiologic conditions (i.e. measured by applying a stress corresponding to an intraocular pressure of 15 mm Hg). However, when measurements were performed at a stress level of 2350 mm Hg (0.31 MPa), the modulus increased dramatically to values between 21 and 57 MPa. We can assume that this trend continues when the stress is increased to stress values such as produced in optical breakdown. Measurement data reported for the ultimate tensile strength of cornea in a direction parallel to the corneal surface range from 3.4 MPa (Duck 1990) to 12.5 MPa (Spörl *et al.* 1996) to 15 MPa (Radt 1997). These values will strongly increase with strain rate (Vogel 1972; Haut 1989; Dombi *et al.* 1993; Vogel & Venugopalan 2003). We can thus conclude that the values used in our numerical calculations are, at least, of the same order of magnitude as the values governing the optical breakdown dynamics in cornea.

A tensile stress wave was also observed after optical breakdown in PAA with 70% water content when large laser pulse energies were used (figure 8). This is, at first sight, surprising because the elastic modulus of this material was experimentally determined to only 0.4 MPa (table 1) while a value of 150 MPa was required to produce a similar behaviour in the numerical calculations. However, it is known that the elastic modulus of polymers dramatically increases with strain rate (Taylor 1946; Kolsky 1949), and the effective elastic moduli of the PAA samples will thus be orders of magnitude larger than the values quoted in table 1. Moreover, it must be noted that in PAA with 70% water content, tensile stress waves could only be produced using fairly large laser pulse energies (10 mJ), and they were weaker than those observed in cornea. We did not use stiffer PAA samples with lower water content in our investigations to obtain a more general occurrence of tensile stress waves, because these samples exhibited an increasingly brittle behaviour. This feature strongly differs from the mechanical properties of strong, collageneous tissues such as cornea or skin. Another possible cause for the disparity of our experimental results for cornea and PAA is the difference in the stress–strain relationships for both materials. Tissues usually become stiffer with increasing stress (Yamada 1970; Vogel & Venugopalan 2003) while the elastic modulus for PAA decreases with increasing load (figure 3).

Delacretaz & Walsh (1997) and Asshauer *et al.* (1997) observed no tensile stress when a cavitation bubble was generated in an aqueous tissue phantom by means of a free-running Holmium laser pulse. When the bubble is produced by a free-running laser pulse, the life cycle of the bubble is comparable to the laser pulse duration, and the bubble growth is driven by the ongoing ablation/vaporization process. The ablation processes in an elastic medium and water thus do not differ very much, and the stress wave formation is also similar in both cases. By contrast, after optical breakdown, the bubble expansion is driven by inertia during most of the bubble lifetime, because the laser pulse duration and the duration of the high initial bubble pressure are much shorter than the oscillation cycle of the bubble. The response to the inertial forces differs strongly for elastic media and water, and the stress wave formation is therefore strongly modified when the breakdown occurs in elastic media.

5.4. *Tissue effects of shock waves and cavitation bubbles*

The primary surgical mechanism of photodisruption is the evaporation of tissue by the laser plasma (Vogel *et al.* 1990, 1996*a*). Collateral effects are mainly mechanical in the form of tissue disruption caused by the stress wave propagation into the tissue and by the cavitation bubble dynamics (Vogel *et al.* 1990, 1996*a*). The stress waves cause damage merely on a cellular and subcellular level which may consist of rupture of cell membranes and injury to cell organelles (Hamrick & Cleary 1968; Watanabe *et al.*

1988; Doukas & Flotte 1996; Lokhandwalla & Sturtevant 2001). Unlike the shock waves, the cavitation bubble dynamics can cause disruptive effects associated with a large tissue displacement, because the bubble becomes much larger than the laser plasma, and its initial expansion velocity is very high during a much longer time than the shock wave duration of the order of 20–150 ns. More detailed discussions of the physical mechanisms of tissue damage by plasma, shock waves, bubble expansion and bubble collapse and the respective histologic findings have been presented elsewhere (Vogel *et al.* 1990, 1994*b*, 1996*a*; Juhasz *et al.* 1994, 1996; Brujan *et al.* 2001*a*), and will not be repeated here. However, we want to emphasize the importance of the different shapes of the stress waves produced by optical breakdown in water and tissues. Purely compressive stress waves such as produced by optical breakdown in water require stress amplitudes of the order of 80–100 MPa and stress gradients of 3–6 MPa ns^{-1} to affect cell viability (Doukas, McAucliff & Flotte 1993; Doukas & Flotte 1996). By contrast, the damage threshold for bipolar stress waves was found to be much smaller, of the order of 10 MPa for the peak tensile stress amplitude (Esenaliev *et al.* 1994), because cells and tissue are more susceptible to tensile stress than to compressive stress.

Tensile stress waves will occur whenever optical breakdown is produced in a tissue structure with large elastic modulus and yield strength. Their damage potential is particularly large when such structures have sensitive cellular structures in their vicinity. This applies, for example, to intrastromal corneal refractive surgery for which laser pulse energies of a few microjoules are employed (Juhasz *et al.* 1999; Heisterkamp *et al.* 2003), and the corneal endothelial cells are located only about 300 μm away from the optical breakdown site. It may be even more important in cutting of hairs mediated by optical breakdown (Optics.Org 2005) because probably larger energies will be required, the tensile stress amplitude is larger (figure 16), and the distance between the breakdown site within the hair and epithelial cells of the hair shaft is less than 100 μm. It must be noted, however, that the prediction of tensile stress amplitudes in subcutaneous laser cutting of hairs is complicated by the fact that breakage of the hair acts like a sudden reduction of the plastic flow stress which will strongly attenuate the tensile component of the emitted stress transient. In femtosecond laser intrastromal refractive surgery no such clipping of the tensile stress is expected. Although only very small laser pulse energies are used, many thousands of pulses must be applied for the generation of a flap for intrastromal excimer laser ablation or the resection of an intrastromal lenticle, and the possibility of cumulative tensile stress effects on the corneal endothelium still remains to be investigated.

6. Conclusions

Stress wave emission and cavitation bubble dynamics after optical breakdown in water and PAA tissue phantoms with Nd:YAG laser pulses of 6 ns duration were investigated experimentally and by numerical simulations. The optical breakdown dynamics was found to depend strongly on the mechanical properties of the surrounding medium, especially on the medium elasticity and the plastic yield strength.

(i) *Cavitation bubble dynamics.* The visco-elastic/plastic behaviour of the tissue phantom leads to a reduction of the maximal bubble size, and a shortening of the oscillation period of the bubble. For very stiff samples, the bubble oscillation is strongly damped. The maximum bubble radius in PAA samples scales with the laser pulse energy in the same way as in water. Well above the breakdown threshold, it is proportional to the cube root of the pulse energy.

(ii) *Stress wave emission during optical breakdown.* Stress waves emitted during optical breakdown in mechanically strong tissues and tissue phantoms are bipolar – a

compressive pulse is followed by a short tensile wave of lower amplitude and a long rarefaction wave exhibiting underpressure but no negative pressure amplitudes. The generation of the tensile stress is related to the shortening of the bubble expansion time and is a consequence of the conservation of momentum. Our numerical simulations revealed that the elastic response of the medium surrounding the bubble is the key feature for the generation of a short tensile stress wave with large amplitude. By contrast, the amplitude of the compressive pulse was found to be largely independent of the mechanical properties of the medium. It is approximately proportional to the square root of the laser pulse energy.

(iii) *Stress wave emission during bubble collapse.* The pressure of the stress wave emitted upon bubble collapse decreases with increasing viscosity, elastic modulus and plastic flow stress of the medium. For soft media (corresponding to PAA samples with 95% water content), the amplitude scaled approximately proportional to $E_L^{0.38}$. For stiff media (corresponding to PAA samples with water content smaller than 80%), no collapse wave was emitted below a critical value of the laser pulse energy.

(iv) *Mechanical properties of PAA and tissue.* Water is a poor model for biological tissues because the shape of the emitted stress waves and the bubble dynamics differ strongly for both materials. PAA is a useful transparent tissue phantom because its mechanical properties can be adjusted by varying the water content, and its melting point is above the boiling point of water. However, the elastic modulus of PAA decreases with increasing strain while it strongly increases in tissues, and the tensile strength of PAA is considerably lower than that of collageneous tissues of equal elastic modulus. Our experimental results for the ultimate tensile strength and flow stress at small and very large strain rates provide evidence that the dynamic mechanical properties relevant for optical breakdown in PAA and tissues may differ by as much as two orders of magnitude from static properties. This conclusion is corroborated by the fact that the values of elastic modulus and flow stress required to reproduce experimental results in numerical simulations were much larger than the static values.

(v) *Implications for laser surgery.* Oscillation of the laser-produced cavitation bubble can produce disruptive effects associated with large tissue displacement while compressive stress effects are mainly on a subcellular level. The discovery of a tensile stress wave after optical breakdown is of great importance for an assessment of collateral damage in plasma-mediated laser surgery because biological tissues are much more susceptible to tensile stress than to compressive stress.

REFERENCES

ASSHAUER, T., DELACRETAZ, G., JANSEN, E. D., WELCH, A. J. & FRENZ, M. 1997 Pulsed holmium laser ablation of tissue phantoms: correlation between bubble formation and acoustic transients. *Appl. Phys.* B **65**, 647–657.

BAREL, A., COURAGE, W. & CLARYS, P. 1995 Suction method for measurement of skin mechanical properties: the Cutometer. In: *Handbook of Non-Invasive Methods and the Skin* (ed. J. Serup & G. B. E. Jemec) CRC Press, Boca Raton.

BRINKMANN, R., HANSEN, CH., MOHRENSTECHER, D., SCHEU, M. & BIRNGRUBER, R. 1996 Analysis of cavitation dynamics during pulsed laser tissue ablation by optical on-line monitoring. *IEEE J. Selected Topics Quantum Electron.* **2**, 826–835.

BRINKMANN, R., THEISEN, D., BRENDEL, T. & BIRNGRUBER, R. 1999 Single-pulse 30-J holmium laser for myocardial revascularization – a study on ablation dynamics in comparison to CO_2 laser-TMR. *IEEE J. Selected Topics Quantum Electron.* **5**, 1–12.

BRUJAN, E. A. 1999 A first-order model for bubble dynamics in a compressible viscoelastic liquid. *J. Non-Newtonian Fluid Mech.* **84**, 83–103.

BRUJAN, E. A., NAHEN, K., SCHMIDT, P. & VOGEL, A. 2001*a* Dynamics of laser-induced cavitation bubbles near an elastic boundary. *J. Fluid Mech.* **433**, 251–281.

BRUJAN, E. A., NAHEN, K., SCHMIDT, P. & VOGEL, A. 2001*b* Dynamics of laser-induced cavitation bubbles near elastic boundaries: Influence of the elastic modulus. *J. Fluid Mech.* **433**, 283–314.

BRUNTON, J. H. 1966 High speed liquid impact. *Phil. Trans. R. Soc. Lond.* A **260**, 79–85.

CHAPYAK, E. J. & GODWIN, R. P. 1998 Physical mechanisms of importance to laser thrombolysis. *Proc. SPIE* **3245**, 12–18.

DELACRETAZ, G. & WALSH, JR, J. T. 1997 Dynamic polariscopic imaging of laser-induced strain in a tissue phantom. *Appl. Phys. Lett.* **70**, 3510–3512.

DOMBI, G. W., HAUT, R. C. & SULLIVAN W. G. 1993 Correlation of high-speed tensile strength with collagen content in control and lathyritic rat skin. *J. Surg. Res.* **54**, 21–28.

DOUKAS, A. G. & FLOTTE, T. J. 1996 Physical characteristics and biological effects of laser-induced stress waves. *Ultrasound Med. Biol.* **22**, 151–164.

DOUKAS, A. G., MCAUCLIFF, D. J. & FLOTTE, T. J. 1993 Biological effects of laser-induced shock waves: structural and functional cell damage in vitro. *Ultrasound Med. Biol.* **19**, 137–146.

DUCK, F. A. 1990 *Physical Properties of Tissue.* Academic.

DYER, P. E., KHOSROSHAHI, M. E. & TUFT, S. J. 1993 Studies of laser-induced cavitation and tissue ablation in saline using a fibre-delivered pulsed HF laser. *Appl. Phys.* B **56**, 84–93.

EBELING, K. J. 1978 Zum Verhalten kugelförmiger, lasererzeugter Kavitationsblasen in Wasser. *Acustica* **40**, 229–239.

EMELIANOV, S. Y., HAMILTON, M. F., ILINSKI, Y. A. & ZABOLOTSKAYA, E. A. 2004 Nonlinear dynamics of a gas bubble in an incompressible elastic medium. *J. Acoust. Soc. Am.* **115**, 581–588.

ESENALIEV, R. O., GOLOVLYOVA, O. A., GOLOVLYOV, V. V. & LETHOKOV V. S. 1994 Effect on erythrocytes of acoustic waves generated upon absorption of laser radiation. *Lasers Life Sci.* **6**, 153–161.

FRENZ, M., KÖNZ, F., PRATISTO, H., WEBER, H. P., SILENOK, A. S. & KONOV, V. I. 1998 Starting mechanisms and dynamics of bubble formation induced by a Ho:Yttrium aluminium garnet laser in water. *J. Appl. Phys.* **84**, 5905–5912.

FRENZ, M., PALTAUF, G. & SCHMIDT-KLOIBER, H. 1996 Laser-generated cavitation in absorbing liquid induced by acoustic diffraction. *Phys. Rev. Lett.* **76**, 3546–3549.

FRIEDMAN, M., STRAUSS, M., AMENDT P., LONDON, R. A. & GLINSKY, M. E. 2002 Two-dimensional Rayleigh model for bubble evolution in soft tissue. *Phys. Fluids* **14**, 1768–1780.

FUNG, Y. C. 1993 *Biomechanics.* Springer.

GLINSKY, M. E., BAILEY, D. S., LONDON, R. A., AMENDT, P. A., RUBENCHIK, A. M. & STRAUSS, M. 2001 An extended Rayleigh model of bubble evolution. *Phys. Fluids* **13**, 20–31.

HAMRICK, P. E. & CLEARY, S. F. 1968 Breakage of tobacco mosaic virus by acoustic transients: a hydrodynamic model. *J. Acoust. Soc. Am.* **45**, 1–6.

HAUT, R. C. 1989 The effects of orientation and location on the strength of dorsal rat skin in high and low speed tensile failure experiments. *Trans. ASME Biomed. Engng* **111**, 136–140.

HEISTERKAMP, A., MAMOM, T., KERMANI, O., DROMMER, W., WELLING, H., ERTMER, W. & LUBATSCHOWSKI, H. 2003 Intrastromal refractive surgery with ultrashort laser pulses: in vivo study on the rabbit eye. *Graefes Arch. Clin. Exp. Ophthalmol.* **241**, 511–517.

HOELTZEL, D. A., ALTMANN, P., BUZARD, K. & CHOE, K. I. 1992 Strip extensiometry for comparison of the mechanical properties of bovine, rabbit, and human corneas. *Trans. ASME* E:*J. Biomech. Engng* **114**, 202–215.

ITH, M., PRATISTO, H., ALTERMATT, H. J., FRENZ, M. & WEBER H. P. 1994 Dynamics of laser-induced channel formation in water and influence of pulse duration on the ablation of biotissue under water with pulsed erbium-laser radiation. *Appl. Phys.* B **59**, 621–629.

ITZKAN, I., ALBAGLI, D., DARK, M. L., PERELMAN, L. T., VON ROSENBERG, C. & FELD, M. 1995 The thermoelastic basis of short pulsed laser ablation of biological tissue. *Proc. Natl Acad. Sci. USA* **92**, 1960–1964.

JANSEN, E. D., ASSHAUER, T., FRENZ, M., MOTAMEDI, M., DELACRETAZ, G. & WELCH, A. J. 1996 Effect of pulse duration on bubble formation and laser-induced pressure waves during holmium laser ablation. *Lasers Surg. Med.* **18**, 278–293.

JUHASZ, T., HU, X. N., TURI, L. & BOR, Z. 1994 Dynamics of shock waves and cavitation bubbles generated by picosecond laser pulses in corneal tissue and water. *Lasers Surg. Med.* **15**, 91–98.

JUHASZ, T., KASTIS, G. A., SUAREZ, C., BOR, Z. & BRON, W. E. 1996 Time-resolved observations of shock waves and cavitation bubbles generated by femtosecond laser pulses in corneal tissue and water. *Lasers Surg. Med.* **19**, 23–31.

JUHASZ, T., LOESEL, F. H., KURTZ, R. M., HORVATH, C., BILLE, J. F. & MOUROU, G. 1999 Corneal refractive surgery with femtosecond lasers. *IEEE J. Selected Topics Quantum Electron.* **5**, 902–910.

KLEIN, M., SCHULTE, H. D. & GAMS, E. 1998 *TMLR Management of Coronary Artery Diseases*. Springer.

KODAMA, T. & TOMITA, Y. 2000 Cavitation bubble behaviour and bubble-shock wave interaction near a gelatin surface as a study of in vivo bubble dynamics. *Appl. Phys. B* **70**, 139–149.

KOLSKY, H. 1949 An investigation of the mechanical properties of materials at very high rates of loading. *Proc. Phys. Soc. B* **62**, 676–700.

KRUEGER, R. R., JUHASZ, T., GUALANO, A. & MARCHI, V. 1998 The picosecond laser for nonmechanical laser in situ keratomileusis. *J. Refract. Surg.* **14**, 467–469.

LAUTERBORN, W., KURZ, T., METTIN, R. & OHL, C. D. 1999 Experimental and theroretical bubble dynamics. In: *Advances in Chemical Physics* (ed. I. Prigogine & S. A. Rice), vol. 110, pp. 295–380.

VAN LEEUWEN, T. G., MEERTENS, J. H., VELEMA, E., POST, M. J. R. & BORST, C. 1993 Intraluminal vapor bubble induced by excimer laser pulse causes microsecond arterial dilatation and invagination leading to extensive wall damage in the rabbit. *Circulation* **87**, 1258–1263.

LESSER, M. B. & FIELD, J. E. 1983 The impact of compressible liquids. *Annu. Rev. Fluid Mech.* **15**, 97–122.

LEVEUGLE, E. & ZHIGILEI, L. V. 2004 Microscopic mechanisms of short pulse laser spallation of molecular solids. *Appl. Phys.* A **79**, 753–756.

LEZZI, A. & PROSPERETTI, A. 1987 Bubble dynamics in a compressible liquid. Part 2. Second-order theory. *J. Fluid Mech.* **185**, 289–321.

LOKHANDWALLA, M. & STURTEVANT, B. 2001 Mechanical haemolysis in shock wave lithotripsy (SWL): I. Analysis of cell deformation due to SWL flow-fields. *Phys. Med. Biol.* **46**, 413–437.

MANSCHOT, J. & BRAKKEE, A. 1986 The measurement and modelling of the mechanical properties of human skin in vivo – I. The measurement. *J. Biomech.* **19**, 511–515.

NICHOLAS, T. & RAJENDRAN, A. M. 1990 Material characterization at high strain rates. In *High Velocity Impact Dynamics* (ed. J. A. Zukas), pp. 127–296. John Wiley & Sons.

NOACK, J. & VOGEL, A. 1998 Single-shot spatially resolved characterization of laser-induced shock waves in water. *Appl. Opt.* **37**, 4092–4099.

NOACK, J. & VOGEL, A. 1999 Laser-induced plasma formation in water at nanosecond to femtosecond time scales: calculation of thresholds, absorption coefficients, and energy density. *IEEE J. Quantum Electron.* **35**, 1156–1167.

OPTICS.ORG 2005 Patent highlights 18 February 2005: a device for shortening hairs by means of laser induced breakdown effects. *International patent application number* WO 2005/011510.

PALTAUF, G. & DYER, P. 2003 Photomechanical processes and effects in ablation. *Chem. Rev.* **103**, 487–518.

PALTAUF, G. & SCHMIDT-KLOIBER, H. 1999 Photoacoustic cavitation in spherical and cylindrical absorbers. *Appl. Phys.* A **68**, 525–531.

RADT, B. 1997 *Mechanical Properties and Thermal Denaturation of Cornea*. Diploma thesis, University of Hamburg and Medical Laser Center Lübeck (in German).

RAYLEIGH, LORD 1917 On the pressure developed in a liquid during the collapse of a spherical cavity. *Phil. Mag.* **34**, 94–98.

SCHOEFFMANN, H., SCHMIDT-KLOIBER, H. & REICHEL, E. 1987 Time-resolved investigations of laser-induced shock waves in water by use of polyvinylidenefluoride hydrophones. *J. Appl. Phys.* **63**, 46–51.

SHEN, Y. R. 1984 *The Principles of Nonlinear Optics*. Wiley.

SIGRIST, M. W. & KNEUBÜHL, F. H. 1978 Laser-generated stress waves in liquids. *J. Acoust. Soc. Am.* **64**, 1652–1663.

SMITH, C. F. 1993 Lasers in orthopedic surgery. *Orthopedics* **16**, 451–534.

SPÖRL, E., GENTH, U., SCHMALFUSS, K. & SEILER, T. 1996 Thermo-mechanical behaviour of the cornea. *Klin. Monatsbl. Augenheilk.* **208**, 112–116 (in German).

STEINERT, R. F. & PULIAFITO, C. A. 1985 *The Nd:YAG Laser in Ophthalmology*. Saunders.

STOLARSKI, D. J., HARDMAN, J., BRAMLETTE, C. G., NOOJIN, G. D., THOMAS, R. J., ROCKWELL, B. A. & ROACH, W. P. 1995 Integrated light spectroscopy of laser-induced breakdown in aqueous media. *Proc. SPIE* **2391**, 100–109.

STRAUSS, M., KAUFMAN, Y., SAPIR, M., AMENDT, P. A., LONDON, R. A. & GLINSKY, M. E. 2002 Self-consistent coupling of cavitation bubbles in aqueous systems. *J. Appl. Phys.* **91**, 4720–4725.

TAYLOR, G. I. 1946 The testing of materials at high rates of loading. *J. Inst. Civil Engng* **26**, 486–518.

TOMITA, Y. & SHIMA, A. 1990 High-speed photographic observations of laser-induced cavitation bubbles in water. *Acustica* **71**, 161–171.

VENUGOPALAN, V., GUERRA, A., NAHEN, K. & VOGEL A 2002 Role of laser-induced plasma formation in pulsed cellular microsurgery and micromanipulation. *Phys. Rev. Lett.* **88**, 078103.

VOGEL, A. & VENUGOPALAN, V. 2003 Mechanisms of pulsed laser ablation of biological tissues. *Chem. Rev.* **103**, 577–644.

VOGEL, A. 1997 Nonlinear absorption: intraocular microsurgery and laser lithotripsy. *Phys. Med. Biol.* **42**, 895–912,

VOGEL, A., HENTSCHEL, W., HOLZFUSS, J. & LAUTERBORN, W. 1986 Cavitation buble dynamics and acoustic transient generation in ocular surgery with pulsed neodymium:YAG lasers. *Ophthalmology* **93**, 1259–1269.

VOGEL, A., SCHWEIGER, P., FRIESER, A., ASIYO, M. & BIRNGRUBER, R. 1990 Intraocular Nd:YAG laser surgery: light–tissue interaction, damage range, and reduction of collateral effects. *IEEE J. Quantum Electron* **26**, 2240–2260.

VOGEL, A., BUSCH, S., JUNGNICKEL, K. & BIRNGRUBER, R. 1994a Mechanisms of intraocular photodisruption with picosecond and nanosecond laser pulses. *Lasers Surg. Med.* **15**, 32–43.

VOGEL, A., CAPON, M. R. C., ASIYO-VOGEL, M. N. & BIRNGRUBER, R. 1994b Intraocular photodisruption with picosecond and nanosecond laser pulses: tissue effects in cornea, lens, and retina. *Invest. Ophthalmol. Vis. Sci.* **35**, 3032–3044.

VOGEL, A., BUSCH, S. & PARLITZ, U. 1996a Shock wave emission and cavitation bubble generation by picosecond and nanosecond optical breakdown in water. *J. Acoust. Soc. Am.* **100**, 148–165.

VOGEL, A., ENGELHARDT, R., BEHNLE, U. & PARLITZ U. 1996b Minimization of cavitation effects in pulsed laser ablation illustrated in laser angioplasty. *Appl. Phys.* B **62**, 173–182.

VOGEL, A., NAHEN K, THEISEN, D. & NOACK, J. 1996c Plasma formation in water by picosecond and nanosecond Nd:YAG laser pulses. Part I: Optical breakdown at threshold and superthreshold irradiance. *IEEE. J. Selected Topics Quantum Electron.* **2**, 847–860.

VOGEL, A., GÜNTHER, T., ASIYO-VOGEL, M. & BIRNGRUBER, R. 1997 Factors determining the refractive effects of intrastromal photorefractive keratectomy with the picosecond laser. *J. Refract. Surg.* **25**, 1301–1310.

VOGEL, A., NOACK, J., NAHEN, K., THEISEN, D., BUSCH, S., PARLITZ, U., HAMMER, D. X., NOOJIN, G. D., ROCKWELL, B. A. & BIRNGRUBER, R. 1999a Energy balance of optical breakdown in water at nanosecond to femtosecond time scales. *Appl. Phys.* B **68**, 271–280.

VOGEL, A., SCAMMON, R. J. & GODWIN, R. P. 1999b Tensile stress generation by optical breakdown in tissue: experimental investigations and numerical simulations. *Proc. SPIE* **3601**, 191–206.

VOGEL, A., SCHMIDT, P. & FLUCKE, B. 2002 Minimization of thermomechanical side effects and increase of ablation efficiency in IR ablation by use of multiply Q-switched laser pulses. *Proc. SPIE* **4617**, 105–111.

VOGEL, H. G. 1972 Influence of age, treatment with corticosteroids and strain rate on mechanical properties of rat skin. *Biochim. Biophys. Acta* **286**, 79–83.

WATANABE, S., FLOTTE, T. J., MCAULIFFE, D. J. & JACQUES, S. L. 1988 Putative photoacoustic damage in skin induced by pulsed ArF excimer laser. *J. Invest. Dermatol.* **90**, 761–766.

YAMADA, H. 1970 *Strength of Biological Materials*. Krieger.